Boehmite Derived γ-Alumina System. 1. Structural Evolution with Temperature, with the Identification and Structural Determination of a New Transition Phase, γ′-Alumina

Gianluca Paglia,[†,‡] Craig E. Buckley,[†] Andrew L. Rohl,[*,‡] Robert D. Hart,[†] Kartsen Winter,[†] Andrew J. Studer,[§] Brett A. Hunter,[§] and John V. Hanna[||]

Departments of Applied Physics and Applied Chemistry, Curtin University of Technology, WA, Perth, 6845, Australia, Bragg Institute and ANSTO NMR Facility, Materials Division, Australian Nuclear Science and Technology Organization, Sydney, NSW, 2234, Australia

Received September 25, 2003. Revised Manuscript Received November 19, 2003

Variations in the structure of gamma-alumina (γ-Al_2O_3), derived from well-crystalline boehmite, calcined at various temperatures in air were investigated. Consistent distribution of cation coordination, ∼69% octahedral and ∼31% tetrahedral, was observed for material calcined between 500 and 900 °C. Gamma alumina was found to be present between 450 and 750 °C. Its structure was tetragonally distorted but showed a reduced tetragonal distortion with increasing temperature. A cubic γ-Al_2O_3 phase was never detected. Above 750 °C, δ-Al_2O_3 was not observed, but instead a new phase was identified and designated gamma-prime-alumina (γ'-Al_2O_3). Similarly to δ-Al_2O_3, γ'-Al_2O_3 was determined to be a triple cell of γ-Al_2O_3 and was described using the $P\bar{4}m2$ space group. The cation ordering in this structure is more obvious than that for γ-Al_2O_3, with fewer site positions being occupied with increasing calcination temperature.

Introduction

Because of its wide range of properties, alumina (Al_2O_3) has enormous technological and industrial significance.[1,2] It exists in a variety of metastable structures including the γ, η, δ, θ, κ, and χ aluminas, as well as its stable α-alumina phase.[3,4] The phase transformations that occur during the calcination of the hydrated alumina phase, gibbsite (γ-$Al(OH)_3$), to α-alumina (α-Al_2O_3) are of fundamental importance in designing ceramic processing procedures, which use partially calcined starting material. The importance of obtaining transition phases in the feedstock for aluminum production, to affect both the adsorption of hydrogen fluoride and the solubility of alumina in the electrolytic solution, is becoming critical.[5−7] The nature of these phase transformations has been studied for many years,[8] and yet there still exists considerable debate over the structures of many of the Al_2O_3 phases. Without adequate knowledge of the structures, research into the properties, dynamics, and applications of these materials will always be less than optimal.

Gamma alumina (γ-Al_2O_3) is reported to occur at temperatures between 350 and 1000 °C.[4,9] It is typically formed from an amorphous or boehmite precursor, and has remained present at temperatures as high as 1200 °C when derived from amorphous aluminas.[10] It occurs in the following transformation sequence:

$$\text{Boehmite/amorphous } Al_2O_3 \rightarrow \gamma\text{-}Al_2O_3 \rightarrow \delta\text{-}Al_2O_3 \rightarrow \theta\text{-}Al_2O_3 \rightarrow \alpha\text{-}Al_2O_3$$

Industrially, γ-Al_2O_3 is an extremely important nanosized material. It has direct application as a catalyst and catalyst support in the automotive and petroleum industries,[11−14] in structural composites for spacecraft,[15]

* To whom correspondence should be addressed. E-mail: andrew@power.curtin.edu.au.
† Materials Research Group, Department of Applied Physics, Curtin University of Technology.
‡ Nanochemistry Research Institute, Department of Applied Chemistry, Curtin University of Technology.
§ Bragg Institute, Australian Nuclear Science and Technology Organization.
|| ANSTO NMR Facility, Materials Division, Australian Nuclear Science and Technology Organization.

(1) Kingery, W. D.; Bowen, H. K.; Uhlmann, D. R. *Introduction to Ceramics*, 2nd ed.; John Wiley and Sons: New York, 1976.
(2) Satterfield, C. N. *Heterogeneous Catalysis in Practice*; McGraw-Hill: New York, 1980; section 4.5.
(3) Stumpf, H. C.; Russell, A. S.; Newsome, J. W.; Tucker, C. M. *Ind. Eng. Chem.* **1950**, *42*, 1398.
(4) Lippens, B. C.; de Boer, J. H. *Acta Crystallogr.* **1964**, *17*, 1312.
(5) Homsi, P. *Third Australasian Smelter Technology Course (Sydney, Australia)*; 1989; p 474.
(6) Hind, A. R.; Bhargava, S. K.; Grocott, S. C. *Colloids Surf., A* **1999**, *146*, 359.
(7) Gillespie, A. R.; Hyland, M. M.; Metson, J. B. *J. Met.* **1999**, *51*, 30.
(8) Zhou, R.-S.; Snyder, R. L. *Acta Crystallogr.* **1991**, *B47*, 617.
(9) O'Connor, B.; Li, D.; Gan, B. K.; Latella, B.; Carter, J. *Adv. X-ray Anal.* **1997**, *41*, 659.
(10) Chou, T. C.; Nieh, T. G. *J. Am. Ceram. Soc.* **1991**, *74*, 2270.
(11) Tung, S. E.; Mcininch, E. *J. Catal.* **1964**, *3*, 229.
(12) Knözinger, H.; Ratnasamy, P. *Catal. Rev. Sci. Eng.* **1978**, *17*, 31.
(13) Taylor, K. In *Catalysis − Science and Technology*; Anderson, J. R., Moudart, M., Eds.; Springer-Verlag: Berlin, 1985; p 119.
(14) Gates, B. C. *Chem. Rev.* **1995**, *95*, 511.
(15) Rosanova, G. G. *12th Annual AIAA/USU Conference on Small Satellites (Logan, Utah, 1998)*; 1998.

10.1021/cm034917j CCC: $27.50
Published on Web 12/30/2003

miniature power supplies,[16,17] and abrasive and thermal wear coatings.[18] γ-Alumina has also been shown to be thermodynamically stable relative to α-Al_2O_3 when a critical surface area is achieved.[19] This outcome can open up endless possibilities for applications of γ-Al_2O_3.

A wide variety of experimental and computational methods have been used to describe the structure of γ-Al_2O_3 over the last half century. However, no definitive consensus has been reached on issues such as the arrangement of vacancies or the role of hydrogen in the structure. The mechanisms by which γ-Al_2O_3 behaves as a catalyst (or support) are not clearly understood. A clear understanding of the structure would assist in elucidating these mechanisms. The many variations of the structure reported are understandable as it has a high degree of disorder and small coherently scattering domain (CSD) sizes, resulting in diffuse diffraction patterns. There are also strong structural similarities to other transition aluminas, observed in the diffraction patterns, which can make it difficult to distinguish between phases in the same transformation sequence.

The structure is traditionally considered to be a cubic spinel type,[20] but it is often reported as tetragonally distorted. When derived from amorphous precursors γ-Al_2O_3 has always been reported as having a cubic lattice.[10,18,21−32] Boehmite-derived γ-Al_2O_3 has been reported as exhibiting a cubic lattice[3,8,33−37] and as having a tetragonal distortion[4,38−44] Regardless of the reports on the tetragonal distortion in its structure, γ-Al_2O_3 has continued to be ascribed the $Fd\bar{3}m$ space group.

The preparation history appears to have important consequences on the type of structure that is produced. Research into the preparation of γ-Al_2O_3 indicates the reaction sequence and kinetics depend on the properties of the precursor.[43−46] This applies not only to different forms of boehmite, such as the gelatinous and highly crystalline types, but also to the conditions under which the boehmite was prepared.

The activation energy for the formation of γ-Al_2O_3 was determined to vary with temperature and pressure in the hydrothermal treatment of boehmite.[44,45] Stumpf et al.[3] determined that heating in a high-pressure environment results in a lower formation temperature for the next transition phase, but as the temperature increases the influence of vapor pressure decreases. Wilson and McConnell[44] suggested that vapor pressure can determine whether intermediate phases in the boehmite to α-Al_2O_3 sequence occur.

Particle size affects the time required for hydrothermal conversion from gibbsite to boehmite.[47,48] However, Gan[49] determined that particle size does not influence the reaction kinetics and pathway from boehmite. Tsuchida et al.[45] and Garn[50] found that the boehmite to γ-Al_2O_3 transformation temperature depends on crystallite size within the particles; larger crystals have higher stability.

Tertian and Papee[39] suggested that the rate of dehydration of boehmite determines the structure, and hence the space group, of the γ-Al_2O_3. They claimed that a slow dehydration rate via a slow heating rate leads to the tetragonally distorted form of γ-Al_2O_3, whereas a more drastic treatment, using a fast heating rate, gives rise to the cubic spinel type γ-Al_2O_3. Wilson,[43,51,52] and Wilson and McConnell,[44] determined that prolonged heating periods resulted in a reduction of the tetragonal distortion of the lattice; it becomes increasingly "cubic". The degree of tetragonal distortion has also been found to decrease with increasing preparation temperature.[42,43] Yanagida and Yamaguchi[42] performed XRD during in situ heating followed by room-temperature measurements and found that the tetragonal distortion was reduced at room temperature.

Tsuchida et al.[45] determined that greater crystallinity of the boehmite precursor leads to tetragonal distortion, signified by more prominent peak splitting about the cubic (400) line. A higher crystalline boehmite also leads to γ-Al_2O_3 of higher crystallinity.[45,53] Splitting about the cubic (400) line becomes obscure for poorly crystalline

(16) Drost, M. K.; Call, C. J.; Cuta, J. M.; Wegeng, R. S. *Microscale Thermophys. Eng.* **1997**, *1*, 321.
(17) Koeneman, P. B.; Busch-Vishniac, I. J.; Wood, K. L. *J. Microelectromech. Sys.* **1997**, *6*, 355.
(18) McPherson, R. *J. Mater. Sci.* **1980**, *15*, 3141.
(19) McHale, J. M.; Navrotsky, A.; Perrotta, A. J. *J. Phys. Chem. B* **1997**, *101*, 602.
(20) Sickafus, K. E.; Wills, J. M.; Grimes, N. W. *J. Am. Ceram. Soc.* **1999**, *82*, 3279.
(21) Verway, E. J. W. *Z. Kristallogr.* **1935**, *91*, 65.
(22) Verwey, E. J. W. *Z. Kristallogr.* **1935**, *91*, 317.
(23) Plummer, M. *J. Appl. Chem.* **1958**, *8*, 35.
(24) Harvey, J.; Mathews, H. I.; Wilman, H. *Discuss. Faraday Soc.* **1960**, *30*, 113.
(25) Dragoo, A. L.; Diamond, J. J. *J. Am. Ceram. Soc.* **1967**, *50*, 568.
(26) McPherson, R. *J. Mater. Sci.* **1973**, *8*, 851.
(27) Dynys, F. W.; Halloran, J. W. *J. Am. Ceram. Soc.* **1982**, *65*, 442.
(28) Morrissey, K. J.; Czanderna, K. K.; Merrill, R. P.; Carter, C. B. *Ultramicroscopy* **1985**, *18*, 379.
(29) Jayaram, V.; Levi, C. G. *Acta Metall.* **1989**, *37*, 569.
(30) Bonevich, J. E.; Marks, L. D. *J. Mater. Res.* **1992**, *7*, 1489.
(31) Ealet, B.; Elyakhloufi, M. H.; Gillet, E.; Ricci, M. *Thin Solid Films* **1994**, *250*, 92.
(32) Levin, I.; Bendersky, D. G.; Brandon, D. G.; Ruhle, M. *Acta Metall.* **1997**, *45*, 3659.
(33) Rooksby, H. *Oxides and Hydroxides of Aluminum and Iron*. In *X-ray Identification and Crystal Structures of Clay Minerals*; Brindley, G. W., Ed.; Mineralogical Society: London, 1961; Chapter 10.
(34) Sinha, K. P.; Sinha, A. P. B. *J. Phys. Chem.* **1957**, *61*, 758.
(35) Liddell, K., PDF 50-0741, JCPDS Database, 1996.
(36) Wang, Y. G.; Bronsveld, P. M.; DeHosson, J. T. M. *J. Am. Ceram. Soc.* **1998**, *81*, 1655.
(37) Wang, J. A.; Bokhimi, X.; Morales, A.; Novaro, O.; Lopez, T.; Gomez, R. *J. Phys. Chem. B* **1999**, *103*, 299.
(38) Saalfeld, H. *Clay Miner. Bull.* **1958**, *3*, 249.
(39) Tertian, R.; Papee, D. *J. Chim. Phys. Phys.−Chim. Biol.* **1958**, *55*, 341.
(40) Saalfeld, H.; Mehrotra, B. *Ber. Deut. Keram. Ges.* **1965**, *42*, 161.
(41) Yanagida, H.; Yamaguchi, G. *Bull. Mater. Sci.* **1962**, *35*, 1896.
(42) Yanagida, H.; Yamaguchi, G. *Bull. Chem. Soc. Jpn.* **1964**, *37*, 1229.
(43) Wilson, S. J. *J. Solid State Chem.* **1979**, *30*, 247.
(44) Wilson, S. J.; McConnell, J. D. C. *J. Solid State Chem.* **1980**, *34*, 315.
(45) Tsuchida, T.; Furuichi, R.; Ishii, T. *Thermochim. Acta* **1980**, *39*, 103.
(46) Wefers, K.; Misra, C. *Oxides and Hydroxides of Aluminum*; Technical Paper 19; Alcoa Laboratories: Pittsburgh, PA, 1987.
(47) Laubengayer, A. W.; Weisz, R. S. *J. Am. Chem. Soc.* **1943**, *65*, 247.
(48) Ervin, G.; Osborn, E. F. *J. Geol.* **1951**, *59*, 381.
(49) Gan, B. K., Crystallographic Transformations Involved in the Decomposition of Gibbsite to Alpha-Alumina. Thesis, School of Physical Sciences, Curtin University of Technology, Perth, Australia, 1996.
(50) Garn, P. D. *Thermoanalytical Methods of Investigation*; Academic Press: New York, 1965; p 95.
(51) Wilson, S. J. *Proc. Brit. Ceram. Soc.* **1979**, *28*, 281.
(52) Wilson, S. J. *Mineral. Magn.* **1979**, *43*, 301.
(53) Abrams, L.; Low, M. J. D. *Ind. Eng. Chem. Prod. Res. Dev.* **1969**, *8*, 38.

precursors.[45] The tetragonal distortion has been attributed to shrinkage anisotropy in the *a* and *b* axes of boehmite during heating,[4] the distribution of residual water or hydroxyl ions,[42] and vacancy ordering on tetrahedral positions.[8,43,44]

It has been shown by electron diffraction that the transformation from boehmite to θ-Al_2O_3 is topotactic. This suggests that there is an orientation relationship of the lattice axes between boehmite and its transition derivatives. The crystals of each polymorph, therefore, exhibit the same shape as their precursor, which is usually sheetlike or lamellar.[4,40,43] As boehmite is heated, its hydroxide layers are destroyed but the oxygen layers remain unaffected, creating the skeleton for γ-Al_2O_3 which converts from hexagonal ABABAB.... stacking to cubic ABCABC... stacking of the oxygen layers.[37] Wilson and McConnell[44] concluded that the transformation sequence from the γ-phase to the θ-phase is energetically favorable due to the structural similarities of the phases concerned. The phases become more ordered with increasing heat treatment.[8]

According to Tertian and Papee,[39] Sato,[54] Lippens and de Boer,[4] and Wilson,[43,51,52] δ-Al_2O_3 occurs as an intermediate between the γ- and θ-polymorphs. However, Saalfeld,[55] Abrams and Low,[53] Zhou and Snyder,[8] Wang et al.,[37] and O'Connor et al.[9] reported no occurrence of the δ-phase. MacKenzie et al.[56] determined that neither δ- nor θ-Al_2O_3 occur when the boehmite precursor is ground before calcination and that grinding led to an increased amorphous content. Despite the ambiguity surrounding the occurrence of a δ-Al_2O_3 intermediate, all of these researchers, with the exception of Abrams and Low[53] and Wang et al.,[37] used similar methods to obtain the boehmite precursor: a pressurized hydrothermal treatment of gibbsite which yields highly crystalline boehmite.

δ-Al_2O_3 derived from boehmite precursors has been described as a triple cell of γ-Al_2O_3, resulting in the appearance of a tetragonal superstructure.[4,43,44,57] Repelin and Husson[57] have reported different *a* and *b* parameters for δ-Al_2O_3 than those that are traditionally believed to be correct, with $a_\delta \approx a_\gamma/\sqrt{2}$, where $a_\gamma \approx 7.9$ Å, and provided a description of the symmetry. These *a* and *b* parameters correspond to those recently determined for γ-Al_2O_3 by Paglia et al.[58] From amorphous precursors, δ-Al_2O_3 has been reported as tetragonal with $c = 1.5a_\gamma$,[59] and with an orthorhombic unit cell.[29]

It was concluded by Wilson and McConnell[44] that there is no distinct difference between δ- and γ-Al_2O_3. This conclusion was supported by the electron energy loss spectroscopy (EELS) of French et al.[60] who found the spectra for the two polymorphs to be almost indistinguishable. The oxygen lattice for γ- and δ-Al_2O_3 are the same; the difference is in the ordering of the Al atoms.[28] It has been suggested that aluminum cation rearrangement occurs, and that vacancies are distributed among octahedral and tetrahedral sites in γ-Al_2O_3, but ordered solely on octahedral sites in δ-Al_2O_3.[36,43,44,57] The tetragonal distortions in γ-Al_2O_3 and δ-Al_2O_3 coincide with vacancy ordering on tetrahedral and octahedral sites, respectively, and the change in the tetragonal distortion relates to the cation migration between the sites.[43,44] Pecharroman et al.,[61] through comparison of infrared (IR) and nuclear magnetic resonance (NMR) spectra of a proven triple cell material (γ-Fe_2O_3) with the spectra of δ-Al_2O_3, suggest the triple-cell hypothesis was not correct and that it can be explained as a mixture of γ- and θ-Al_2O_3.

The work presented here follows from similar work done previously within our research group[9,49] in which the transformation pathways from gibbsite to α-Al_2O_3 were examined. Part of that work also involved examining the evolution of γ-Al_2O_3 with increasing calcination temperature using neutron diffraction. A novel description was offered in that γ-Al_2O_3 was a dual-phase material, consisting of both cubic and tetragonal γ-Al_2O_3, which coexist at all temperatures between 400 and 900 °C. The tetragonal structure was suggested to dominate at lower temperatures, with the cubic phase becoming dominant from 750 °C onward.

In previous work, we determined a model which describes tetragonally distorted boehmite-derived γ-Al_2O_3 using the tetragonal $I4_1/amd$ space group, rather than $Fd\bar{3}m$.[58] It was also demonstrated that an accurate average structural model cannot be achieved if the cations are restricted to spinel positions. Vacancies were determined to be distributed among both tetrahedral and octahedral sites. The results also suggested that hydrogen is not present interstitially within the crystalline bulk structure, but rather exists in the form of water within the amorphous content. The tetragonal structural model for γ-Al_2O_3 was determined for a single temperature case. This paper considers γ-Al_2O_3 derived from a highly crystalline boehmite precursor by investigating the evolution of the bulk structural configuration of boehmite calcined in air at various temperatures. The identification and determination of a new phase is also shown.

Experimental Section

Materials. Powdered γ-Al_2O_3 was obtained from two highly crystalline boehmite precursors and used for neutron studies. Hydrogenated boehmite was obtained from the Alumina and Ceramics Laboratory, Malakoff Industries (Bauxite, AR). Deuterated boehmite was prepared by hydrothermal treatment of Alcoa C31 hydrogenated gibbsite with D_2O for 10 days at 158 °C in a Barc bomb (~150 kPa pressure). Each boehmite precursor was calcined at temperatures between 400 and 1000 °C, at 50 ± 5 °C intervals, in air. The heating rate was 5 °C per minute. Calcination of each sample lasted for 7 h at each temperature. In the case of one hydrogenated sample, calcination proceeded for 13 h at each temperature. After calcination the furnace was switched off and each sample was allowed to cool to room temperature.

Neutron Diffraction. Neutron diffraction data were collected in-situ during calcination using the medium-resolution powder diffractometer (MRPD) with a 1.66 Å wavelength, at the high-flux Australian reactor (HIFAR) operated by the

(54) Sato, T. *J. Appl. Chem.* **1962**, *12*, 9.
(55) Saalfeld, H. *Neues Jahrb. Mineral. Abh.* **1960**, *95*, 1.
(56) MacKenzie, K. J. D.; Temuujin, J.; Smith, M. E.; Angerer, P.; Kameshima, Y. *Thermochim. Acta* **2000**, *359*, 87.
(57) Repelin, Y.; Husson, E. *Mater. Res. Bull.* **1990**, *25*, 611.
(58) Paglia, G.; Buckley, C. E.; Rohl, A. L.; Hunter, B. A.; Hart, R. D.; Hanna, J. V.; Byrne, L. T. *Phys. Rev. B* **2003**, *68*, 141110.
(59) Rooksby, H. P.; Rooymans, C. J. M. *Clay Miner. Bull.* **1961**, *4*, 234.
(60) French, R. H.; Mullejans, H.; Jones, D. J. *J. Am. Ceram. Soc.* **1998**, *81*, 2549.
(61) Pecharroman, C.; Sobrados, I.; Iglesias, J. E.; Gonzales-Carreno, T.; Sanz, J. *J. Phys. Chem. B* **1999**, *103*, 6160.

Australian Nuclear Science and Technology Organization (ANSTO), Lucas Heights Laboratories, Sydney, Australia. The in situ data were collected at the selected temperatures in hourly intervals, yielding one complete neutron diffraction pattern every hour over the duration of calcination, so that kinetic effects could be investigated. Neutron diffraction data, using MRPD and the high-resolution powder diffractometer (HRPD) were also obtained at room temperature from precalcined samples prepared from hydrogenated boehmite under the conditions specified above. A wavelength of 1.49 Å was used for the HRPD experiments.

Rietveld Analysis and the Starting Structure Models. Rietveld analysis[62,63] of the neutron diffraction data from powdered γ-Al_2O_3 was performed using the LHPM Rietveld code with the Rietica 1.7.7 interface.[64]

Three structural models were used in Rietveld refinements of the neutron diffraction data. The quality of the fit of the refined structure models to the data was determined visually by inspection of the residual plot and statistically by figures-of-merit of the estimated standard deviation of individual parameters. The figures-of-merit provided here are the profile factor (R_p), "goodness-of-fit" (χ^2), and "Bragg factor" (R_B).[65]

Nuclear Magnetic Resonance. ^{27}Al MAS NMR spectra were recorded at ambient temperature for the samples obtained at 500, 600, 700, 800, and 900 °C from hydrogenated boehmite. The spectra were determined using a Bruker MSL-400 spectrometer (9.4 T) operating at a ^{27}Al frequency of 104.23 MHz. The solid sample was spun around an axis inclined at 54°44′ (the magic angle) with respect to the magnetic field, at a rate of 15 kHz using a Bruker 4-mm double-air-bearing probe. Each MAS NMR spectrum was obtained after a 3 μs 90 and a 0.6 μs 90 pulse length on the solution and sample, respectively. A 1.0 M $Al(NO_3)_3$ solution was employed as the chemical shift reference (set to 0.0 ppm), and for calibrating the experimental pulse lengths.

The baseline of the MAS NMR spectra were corrected before peak integration and peak deconvolution to obtain the coordination distribution of Al. This baseline correction was repeated 20 times on each spectrum to obtain an indication of its contribution to the uncertainty in the measurements.

Transmission Electron Microscopy. Dispersed samples of hydrogenated γ-Al_2O_3 on carbon film were investigated using a JEOL 2011 transmission electron microscope (TEM) fitted with a LaB_6 filament and operated at 200 kV. Selected area electron diffraction (SAED) patterns were obtained using a 1500-mm camera length. The camera length was calibrated by comparison with diffraction patterns from pure gold. The absence of kikuchi bands, attributable to the disorder in the structure, made it difficult to discern zone axes and thus difficult to obtain useful information using convergent-beam electron diffraction (CBED).

Thermal Analysis. Thermogravimetric analysis (TGA) and differential thermal analysis (DTA) were employed to provide, respectively, (i) details on weight loss with temperature due to dehydration of the transition aluminas from the starting material gibbsite, and (ii) to extract endothermic and exothermic details such that the temperatures at which transitions occur can be determined.[66] Experiments were performed with a Stanton Red-Croft model STA 780 simultaneous DTA−TGA machine. Approximately 15 mg of material was placed in an alumina crucible with a height of 3.0 mm and an internal diameter of 3.8 mm. The sample was then heated in air (flow rate = 35 mL min^{-1}) from room temperature to 1300 °C. The heating rate was 20 °C min^{-1}.

X-ray Diffraction. X-ray diffraction (XRD) data were also obtained at room temperature for the hydrogenated boehmite samples which had been precalcined at 50 °C intervals between 400 and 1000 °C. The XRD data were collected with a Siemens D5OO Bragg−Brentano instrument, using collimated Cu Kα (λ = 1.5418 Å) monochromatic radiation. The 2θ range employed was 10 to 70°, with a 0.05° step size.

Results and Discussion

DTA−TGA analysis of a hydrogenated boehmite sample (Figure 1a) shows an endotherm at ∼542 °C, which corresponds to the lattice changes coinciding with the transformation of boehmite to γ-Al_2O_3.[46,49] A total of ∼16 wt. % was lost during the whole scan, the majority of which occurred with the formation of γ-Al_2O_3. The TGA curve shows a less significant loss of mass, before the major downward slope, between 400 and 500 °C, corresponding to the onset of transformation. DTA−TGA was performed on a deuterated boehmite sample also and exhibited a similar mass loss of ∼17 wt. % during the whole scan. The endotherm, representing the transformation to γ-Al_2O_3 occurred at a slightly lower temperature of ∼529 °C. Particle size appears to be the most obvious factor in the temperature differences, with the mean particle sizes being ∼16 μm and ∼4 μm for the hydrogenated and deuterated boehmite, respectively. Beyond the conversion to γ-Al_2O_3 there are no endotherms indicating transformation to other phases and almost negligible mass loss.

The relative scale of the endotherm, and corresponding mass loss, (Figure 1a) makes it difficult to see events which occur beyond the transformation to γ-Al_2O_3. Hence, DTA−TGA analysis was performed on a hydrogenated γ-Al_2O_3 sample calcined at 600 °C (Figure 1b). The endotherm at ∼52 °C and mass loss to ∼450 °C correspond to the loss of surface adsorbed water. A second endotherm at ∼1161 °C and mass loss of ∼2.8 wt. % corresponds to the formation of α-Al_2O_3. Preceding this temperature, there are no endotherms indicative of significant lattice changes. However, there are small inflection points in the TGA curve at ∼750 and 950 °C, which coincide with the approximate formation temperatures expected for the δ- and θ-phases.[46]

The differences between in situ neutron diffraction data obtained at each calcination temperature were examined to investigate at which temperatures lattice changes occur. This was accomplished by subtracting the neutron diffraction data collected in hourly intervals from the data collected during the final hour of calcination to yield a difference plot (Figure 2). Asymmetric spikes in the difference plot signify structural changes in the material.

The neutron data showed that conversion of boehmite to γ-Al_2O_3 was complete by 500 °C. Difference plots indicated that the greatest lattice changes during the whole calcination period occurred at 450 °C for both the hydrogenated and deuterated samples, indicating the phase transformation. For the deuterated boehmite, the onset of phase transformation occurred at 400 °C with minor asymmetric spikes being observed. The earlier onset of phase transformation for neutron diffraction data may be explained by the slower heating rate and more prolonged heating times compared to those of the DTA−TGA. For DTA−TGA, the entire scan was achieved in approximately 1 h.

The difference plots showed no further lattice changes beyond 450 °C until 900 °C for the deuterated boehmite

(62) Rietveld, H. M. *J. Appl. Crystallogr.* **1969**, *2*, 65.
(63) Young, R. A., Ed. *The Rietveld Method*; International Union of Crystallography, Oxford University Press: New York, 1993.
(64) Hunter, B. A. *IUCr Comm. Powder Diffraction Newsletter* **1998**, 20, article 16.
(65) Young, R. A.; Wiles, D. B. *J. Appl. Crystallogr.* **1982**, *15*, 430.
(66) Pope, M. I.; Judd, M. D. *Differential Thermal Analysis*; Heyden and Son Ltd.: London, 1977.

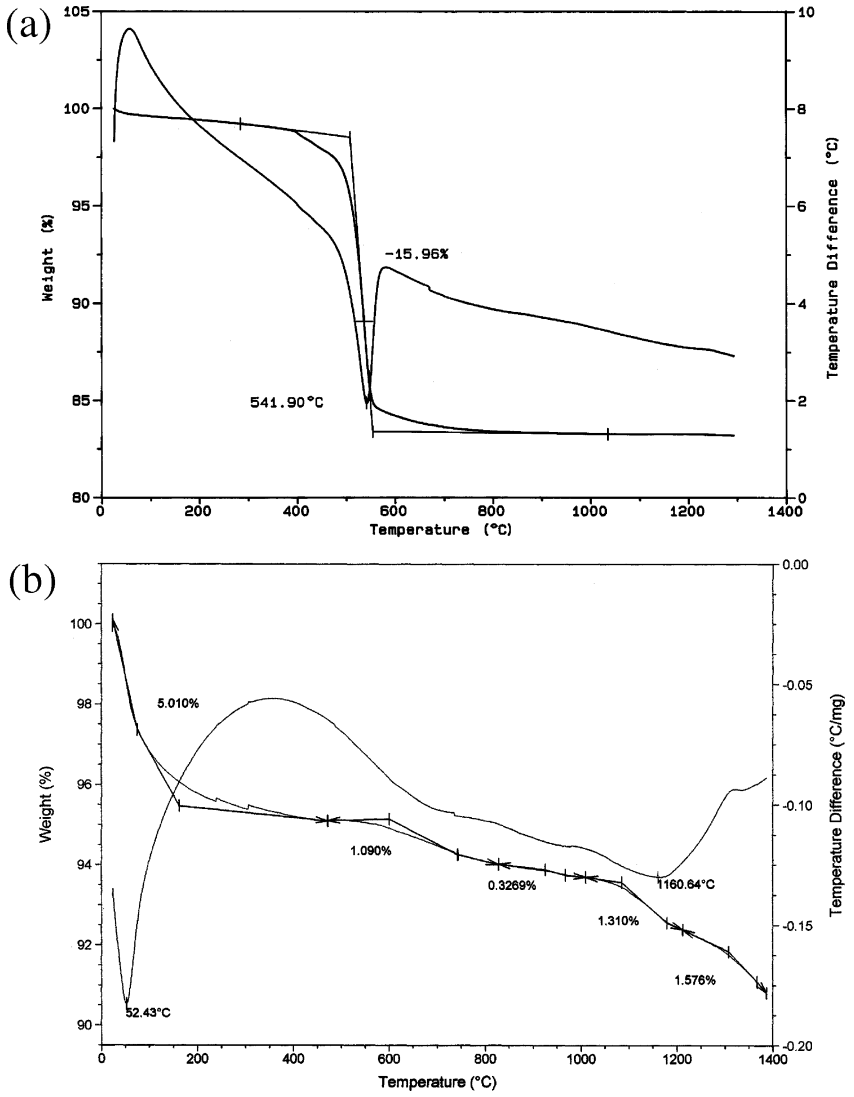

Figure 1. DTA−TGA results for (a) hydrogenated boehmite, and (b) the γ-Al_2O_3 sample resulting from the calcination of hydrogenated boehmite at 600 °C.

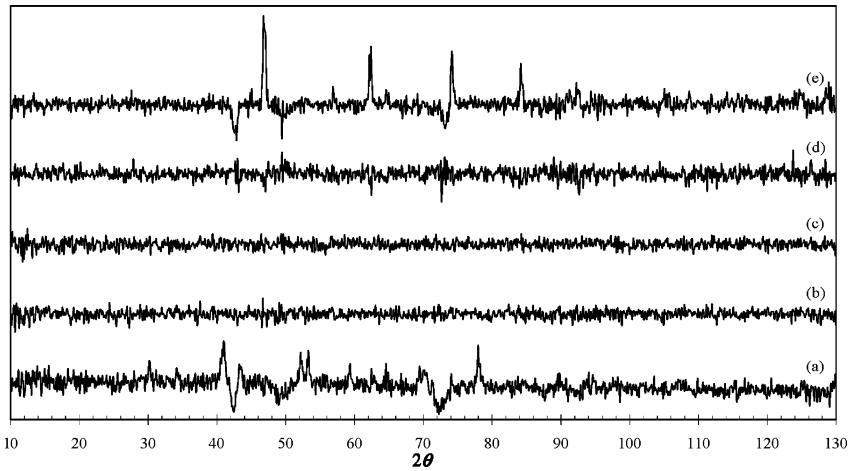

Figure 2. Example difference plots from neutron diffraction data collected in situ during calcination, of deuterated boehmite precursor, at (a) 450, (b) 500, (c) 700, (d) 900, and (e) 950 °C.

and 950 °C for the hydrogenated boehmite. The changes at these temperatures were marginal and become more significant at higher temperatures. These higher-temperature lattice changes correspond to the onset of formation of θ-Al_2O_3. It was therefore decided to further investigate the structures between 500 and 900 °C.

For all temperatures between 500 and 900 °C no kinetic effects were observed after the first half hour of calcination. This was confirmed by Rietveld refinements of hourly data sets, which showed negligible change in the lattice parameters and unit cell coordinates for the duration of calcination at each of these temperatures.

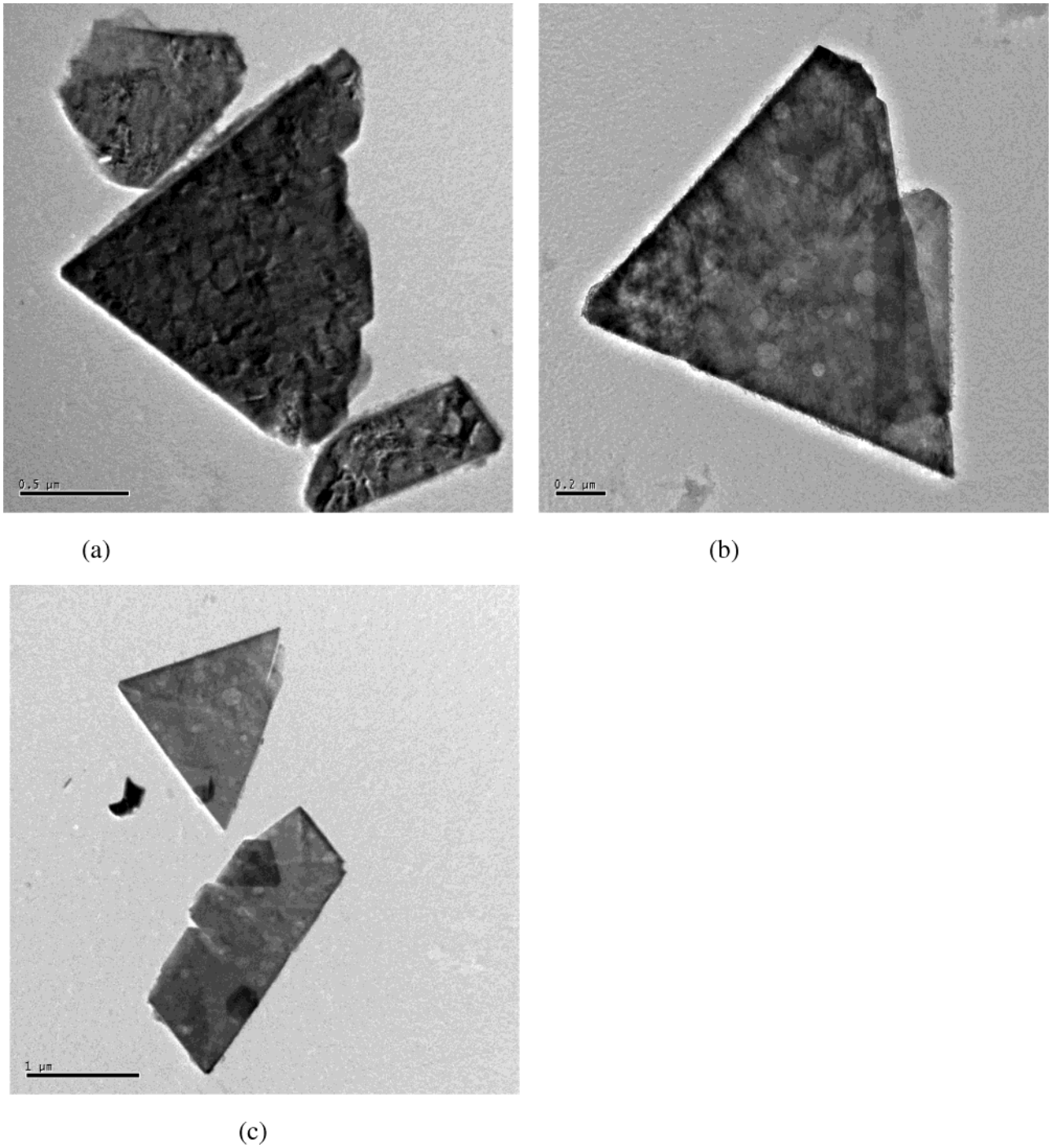

Figure 3. Examples of grain shapes: (a) boehmite, (b) γ-Al_2O_3 formed from boehmite calcined at 500 °C, (c) γ-Al_2O_3 formed from boehmite calcined at 600 °C.

This allowed for the addition of multiple hourly data sets to yield better statistics for the structure determinations by Rietveld refinement.

Morphology of Samples. The samples exhibited a platelike morphology similar to that observed by previous researchers.[67,68] The plates had triangular-, rectangular-, and rhombic-type morphologies and ranged between 0.1 and 4 μm along the longest dimension, with thicknesses between 0.1 and 0.6 μm for the larger grains (Figure 3). These plates are not single crystals; they are grains composed of lamellar crystallites.[43,51,52] Rietveld analysis, assuming ellipsoid crystallites, returns dimensions between 100 and 800 Å. It has been determined that the differences between the data and the calculated patterns mentioned in our previous work,[58] particularly at $2\theta \approx 44°$, the (220) direction, results from the inadequacy of currently available profile functions to model the crystallite shapes and sizes characteristic of these materials. Although there has recently been promising research to overcome these difficulties,[69,70] the available Rietveld codes still do not accommodate the inherent anisotropic broadening due to stacking faults and anisotropic strain. The discrepancy between the data and the calculated pattern was found for all

(67) Wilson, S. J.; McConnell, J. D. C.; Stacey, M. H. *J. Mater. Sci.* **1980**, *15*, 3081.
(68) Souza Santos, P.; Souza Santos, H. S.; Toledo, S. P. *Mater. Res.* **2000**, *3*, 104.

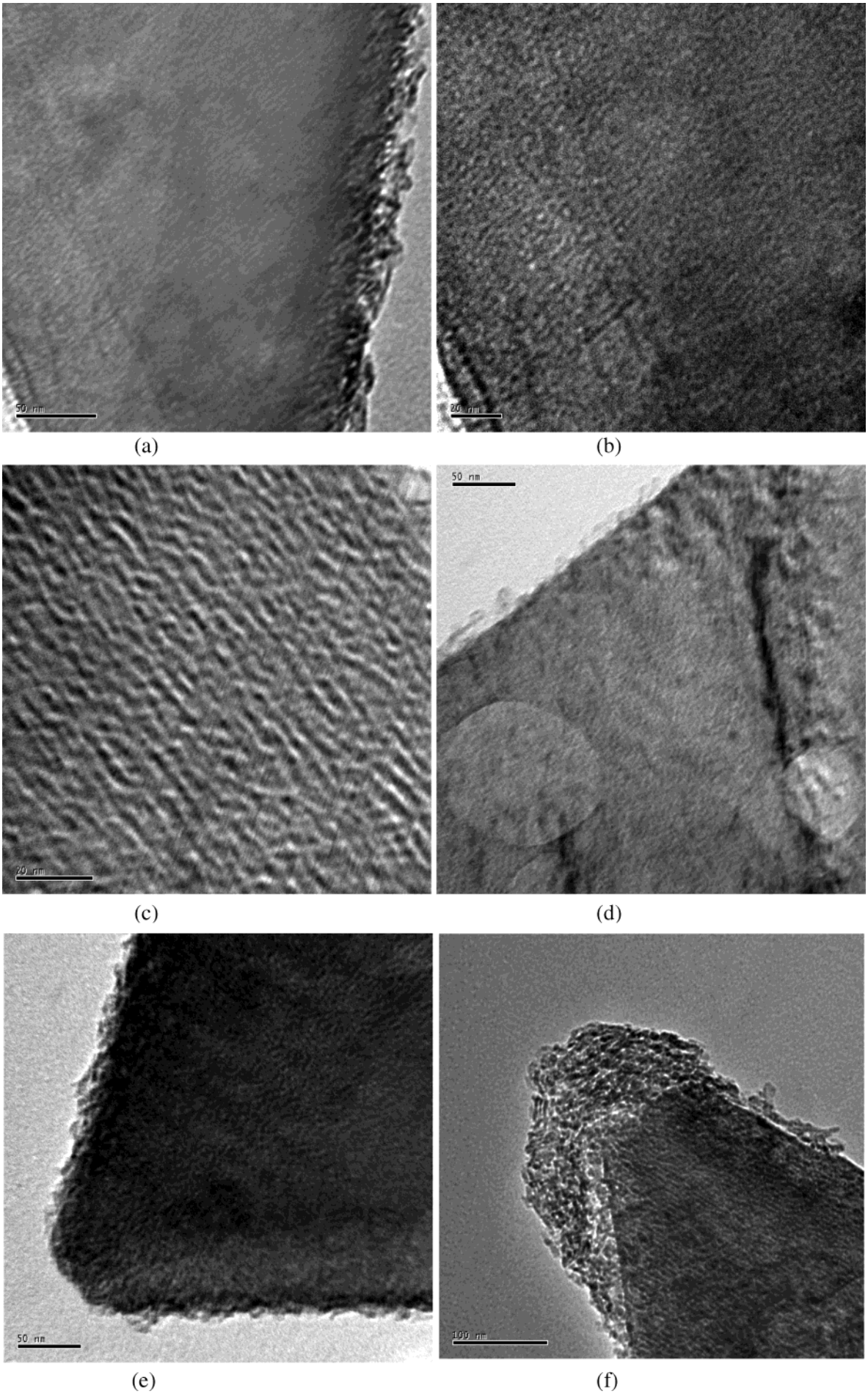
50 nm
20 nm
(a)
(b)
20 nm
50 nm
(c)
(d)
50 nm
100 nm
(e)
(f)

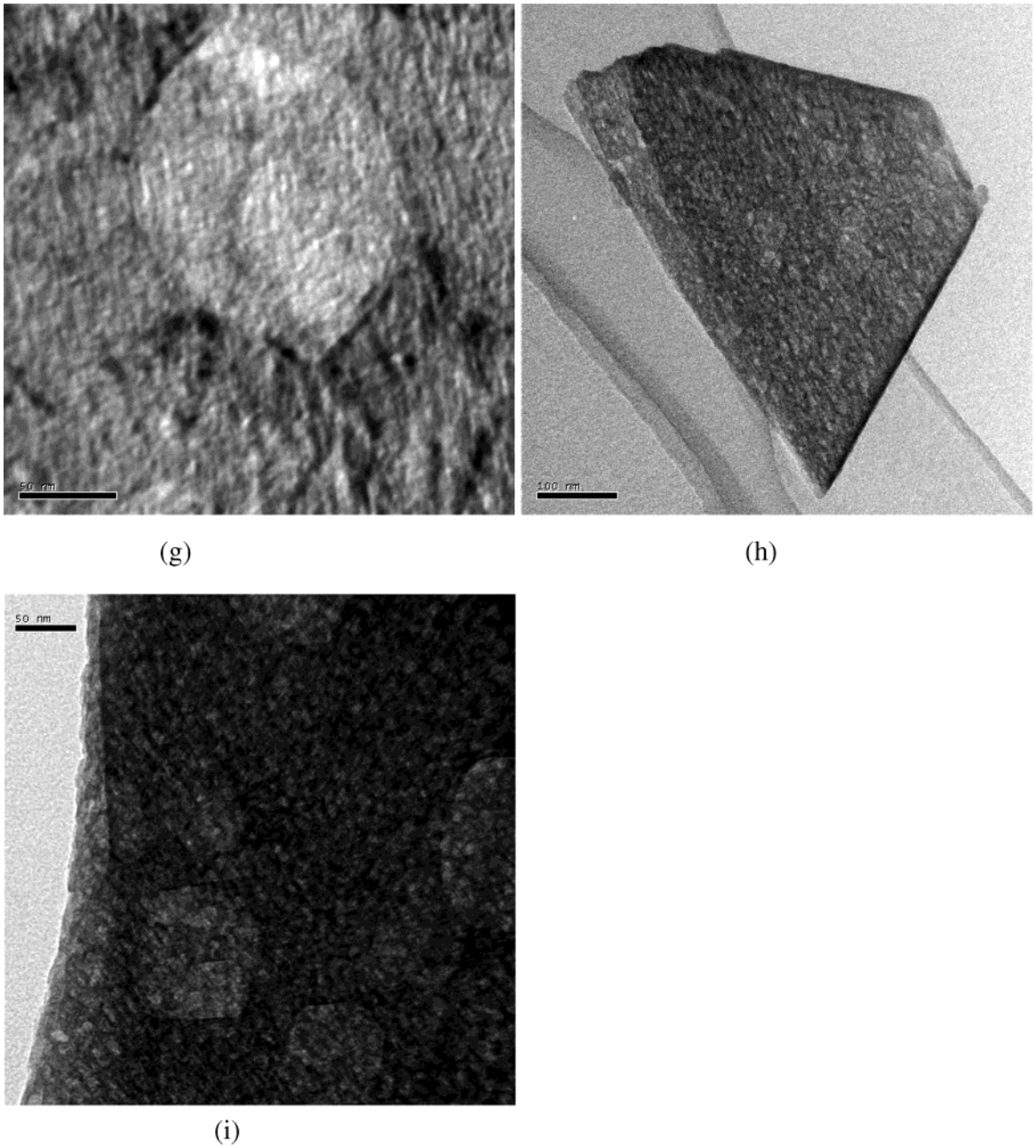

Figure 4. Examples of microstructure: (a) and (b) boehmite; (c) and (d) γ-Al_2O_3 formed from boehmite calcined at 500 °C; (e) and (f) γ-Al_2O_3 formed from boehmite calcined at 600 °C; (g) γ-Al_2O_3 formed from boehmite calcined at 700 °C; and (h) and (i) γ'-Al_2O_3 formed from boehmite calcined at 900 °C.

data sets examined by Rietveld refinement at every calcination temperature. As a result, the Scherrer equation, which ignores strain, was manually applied to the full-width-half-maximum, determined by Warren's method, of the only nonoverlapping peak, at $2\theta \approx 44°$, yielding an average crystallite size of ~150 Å for all samples calcined to and including 750 °C, ~185 Å for samples calcined to 800 °C, and ~210 Å for samples calcined at 900 °C. TEM images of γ-Al_2O_3 where material appears to be decomposing at the edges of the grain, due to the electron beam intensity, indicate crystallite sizes up to 300 Å. Most crystallites appeared to be rectangular but some looked spherical.

Most of the grains were composed of multiple sheet-like layers. Overlapping SAED patterns, and CBED patterns that "wobbled" as the beam was moved over individual grains, provided further evidence of this. It was difficult to find isolated grains which were not layered. Twinning of the grains was observed ubiquitously throughout the samples and this was also reflected in the SAED patterns. The layered nature of the grains and their twinning made it difficult to obtain nonoverlapping diffraction patterns. Smaller grains tended to become unstable under the beam. The electron beam was found to cause lattice expansion in γ-Al_2O_3 when focusing for diffraction. Deliberate heating from the beam in the high vacuum environment caused fast dehydration of boehmite to form γ-Al_2O_3 as seen by previous researchers.[43,71]

(69) Balzar, D.; Von Dreele, R. B.; Bennett, K.; Ledbetter, H. *J. Appl. Phys.* **1998**, *84*, 4822.
(70) Stephens, P. W. *J. Appl. Crystallogr.* **1999**, *32*, 281.

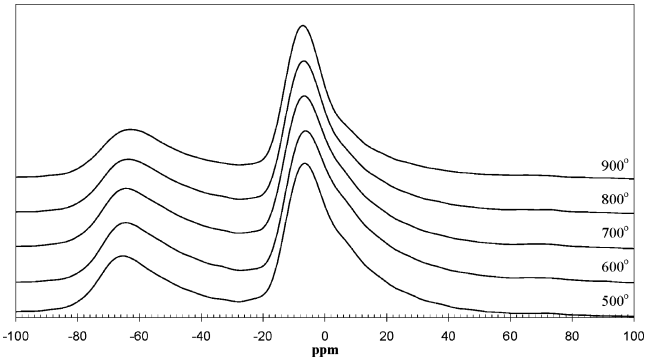

Figure 5. MAS NMR spectra for γ-Al_2O_3 prepared from hydrogenated boehmite precursor, calcined between 500 and 900 °C.

The platelike shapes of all calcination products are consistent with the boehmite precursor (Figure 3), until the formation of θ-Al_2O_3, indicating phase transformations within isovolumetric environments. This confirms the topotactic nature of the transformation from boehmite to θ-Al_2O_3 suggested by earlier researchers.[4,40,43]

A lamellar porous microstructure, similar to that observed by Wilson,[43,51,52] Wilson et al.,[67] and Lippens and De Boer,[4] was observed for the calcination products (Figure 4). This is in contrast to the more ordered and featureless microstructure of boehmite. Hexagonal facets, much larger than those observed by others,[71,72] were observed on the surface of all calcination products. The calcination products obtained over 800 °C showed more microstructure ordering than those obtained between 500 and 700 °C. Regions of dark contrast were observed intermittently within the grains (Figure 4d and g). Their occurrence is reduced with increasing calcination temperature and we believe they correspond to the location of amorphous content. Bulk structure hydrogen is likely to reside within these regions.[58,73]

Wilson and McConnell[44] found no obvious variations in the microstructure of γ-Al_2O_3 (and δ- or θ-Al_2O_3) samples, compared with other samples of the same phase, prepared under different conditions from the same well-crystalline boehmite precursor, calcined in air. The morphological TEM analysis performed here concurs with these findings, with no obvious differences in microstructure being observed for the calcination products obtained between 500 and 700 °C or the calcination product obtained between 800 and 900 °C.

Unlike the microstructure, diffraction patterns exhibited different characteristics for each calcination temperature within these ranges. However, the diffraction patterns did display the same features at each particular calcination temperature for material prepared by different preparation routes from identical precursor.

Structural Variation with Temperature and the Identification of a New Phase: γ'-Alumina. MAS NMR spectra of the hydrogenated samples of γ-Al_2O_3 (Figure 5) calcined between 500 and 900 °C appear identical for each temperature. As per our previous study,[58] no peaks representative of pentahedrally coordinated cations were observed. The asymmetric tailing of the peaks, indicative of short-range disorder in the structure, was consistent for all temperatures.[74−78] The cation coordination, from peak integration, was determined to be nearly identical for each sample. The 500 °C data yielded a coordination distribution of 68(2)% octahedral and 32(2)% tetrahedral for the Al cations. Data for the remaining calcination temperatures yielded a coordination distribution of 69(2)% octahedral and 31-(2)% tetrahedral for the Al cations. As temperature increases, the octahedral sites are expected to become less occupied, particularly after 750−800 °C where the formation of δ-Al_2O_3 is anticipated.[28,36,57] The model for δ-Al_2O_3 given by Repelin and Husson[57] indicates that ~38% of the cations are situated in tetrahedral positions, higher than the values shown in the MAS NMR data here.

XRD patterns measured at room temperature (Figure 6) show that γ-Al_2O_3 is present for material calcined between 500 and 700 °C. It can be seen that the peak at 2θ ~46° (004) is split at 500 °C, indicating the tetragonal nature of the structure. The peaks at 2θ ~39° and 65° also exhibit splitting. The degree of splitting becomes visibly reduced up to 700 °C, coinciding with a decrease in the tetragonal nature of γ-Al_2O_3 with increasing temperature. However, a cubic γ-Al_2O_3 structure was not observed for the samples examined here. For material calcined at 800 °C the peak splitting at 2θ ~46 ° becomes more pronounced again, concurrent with an increase in tetragonal distortion. This coincides with the appearance of more peaks as the calcination temperature increases to 900 °C, which have been labeled in Figure 6 with a γ' symbol. The trend of the reduced tetragonal distortion up to 700 °C, and its increase for higher calcination temperatures, is similar to the observations of Wilson, Wilson and McConnell, and Gan.[9,43,44,49] The diffraction patterns above 800 °C are clearly not characteristic of δ-Al_2O_3.[57] However, it is also clear that the structure is not γ-Al_2O_3, although the patterns maintain characteristics similar to those of γ-Al_2O_3. We conclude that this is a new phase, which we have designated γ'-Al_2O_3. It occurs in place of δ-Al_2O_3, between γ and θ-Al_2O_3, in the transformation sequence for the material examined here.

Similar variations in the diffraction patterns are observed for neutron data. Figure 7 shows neutron diffraction patterns of hydrogenated boehmite calcined between 500 and 900 °C. Higher background contributions are characteristic of the data between 500 and 600 °C (although not clear from Figure 7). The background is significantly flatter at 650 °C, suggesting reduced amorphous content. Beyond 700 °C, there was little change in the background of each neutron diffraction pattern. The tetragonal nature, signified by split peaks, is still evident at 700 °C. At 750 °C the sample is still considered to be γ-Al_2O_3. However, instead of a reduced

(71) Kogure, T. *J. Am. Ceram. Soc.* **1999**, *82*, 716.
(72) Kryukova, G. N.; Klenov, D. O.; Ivanova, A. S.; Tsybulya, S. V. *J. Eur. Ceram. Soc.* **2000**, *20*, 1187.
(73) Paglia, G.; Buckley, C. E.; Rohl, A. L.; Jones, F.; Udovic, T. J.; Maitland, C. F.; Connolly, J.; submitted for publication.
(74) Phillips, B. L.; Kirkpatrick, R. J.; Hovis, G. L. *Phys. Chem. Miner.* **1988**, *16*, 262.
(75) Kohn, S. C.; Dupree, R.; Smith, M. E. *Geochim. Cosmochim. Acta* **1989**, *53*, 2925.
(76) Kohn, S. C.; Dupree, R.; Mortuza, M. G.; Henderson, C. M. B. *Am. Miner.* **1991**, *76*, 309.
(77) Kunath, G.; Losso, P.; Schneider, H.; Steurnagel, S.; Jäger, C. *Solid State Nucl. Magn. Reson.* **1992**, *1*, 261.
(78) Kunath-Fandrei, G.; Bastow, T. J.; Hall, J. S.; Jäger, C.; Smith, M. E. *J. Phys. Chem.* **1995**, *99*, 15138.

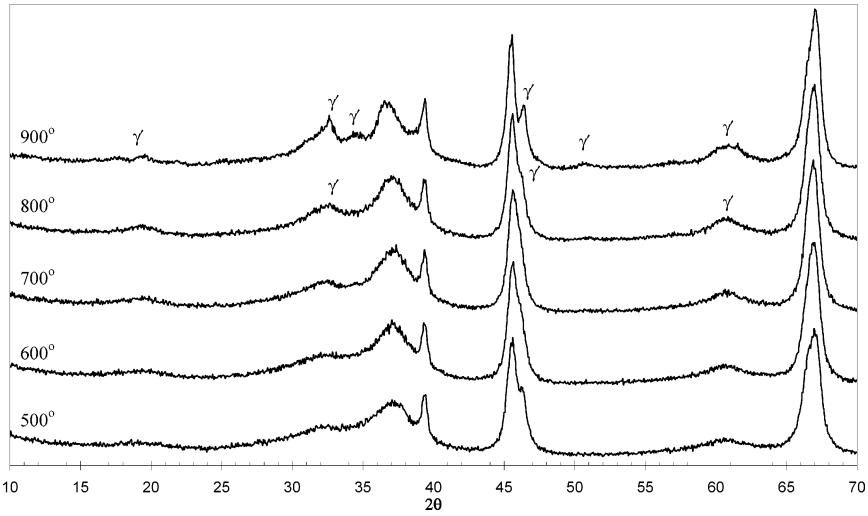

Figure 6. XRD patterns for γ-Al_2O_3 prepared from hydrogenated boehmite precursor, calcined between 500 and 900 °C.

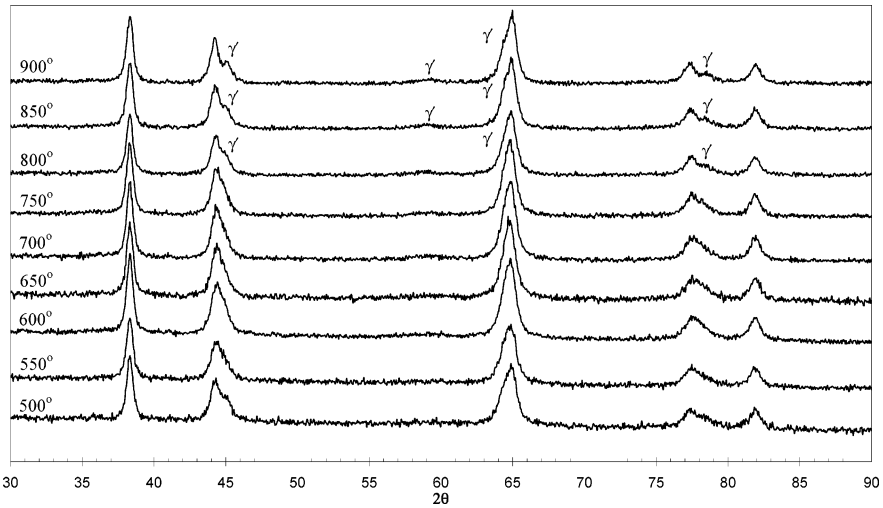

Figure 7. HRPD neutron diffraction patterns for hydrogenated boehmite precalcined for 7 h at temperatures between 500 and 900 °C.

tetragonal profile at $2\theta \sim 44$ °, the peak is once more increasingly split. This represents the initial formation of the first γ'-Al_2O_3 peak. The same trends were observed for all neutron data collected, both at room temperature and while heating in situ. The only exception is that γ'-Al_2O_3 is clearly formed at 750 °C for the deuterated boehmite precursor instead of at 800 °C.

The continuous change in the diffraction patterns with increasing temperature, the absence of lattice changes in difference plots, the consistency between room temperature and in situ data, and the lack of endotherms with marginal mass losses in DTA−TGA curves after the formation of γ-Al_2O_3 suggest a higher-order phase transformation. This implies continuous variation of the sub-cell parameters in the transformation from γ-Al_2O_3.[44]

The higher-order phase transformation is directly evident from SAED patterns (Figure 8), which show increased streaking with increased calcination temperature between 500 and 700 °C, as shown by the streaking about the *hkl*: $h + k + l = 2n$ reflections, e.g., (200). At 700 °C, two peaks can be seen at the extremities of the streak about (200). By 800 °C the reflections exhibit the same characteristics as the lower-temperature diffraction patterns. However, additional reflections have appeared and a new symmetry-reduced unit cell comprising a triple cell of the original γ-Al_2O_3 unit cell is suggested. The (200) reflection, no longer a defined peak, has split into two (202) peaks of the new γ'-Al_2O_3 phase. By 900 °C the triple cell is the same as that at 800 °C but what was once streaking about the (200) reflection has almost disappeared and the *h*0*l*: $h + l =$ *even* reflections of the γ'-Al_2O_3 phase, e.g. (109), show increased streaking and splitting into multiple peaks. The diffraction pattern at 900 °C shows some characteristics of a δ-Al_2O_3 pattern.

Figure 9 shows the indexing diagrams for γ-Al_2O_3 and γ'-Al_2O_3. The diffraction patterns were obtained down the [0*k*0] zone axis. Diffraction patterns down the [00*l*] zone axis could not be obtained as a tilt rotate stage was unavailable.

Lippens and de Boer[4] showed there are three types of reflections for γ-Al_2O_3.[4] The most diffuse or streaked, the *hkl*: $h + k + l = 2n$ reflections, represent planes with Al cations in tetrahedral positions. The sharpest and most intense peaks, the *hkl*: $h + k + l = 4n$ reflections, e.g., (400) and (202), originate from planes with both cations and oxygens. The final type of reflection originates from planes with octahedrally and tetrahedrally coordinated cations. The *h*0*l*: $h + l =$ *even* reflections, e.g., (103), are of this type. These are more

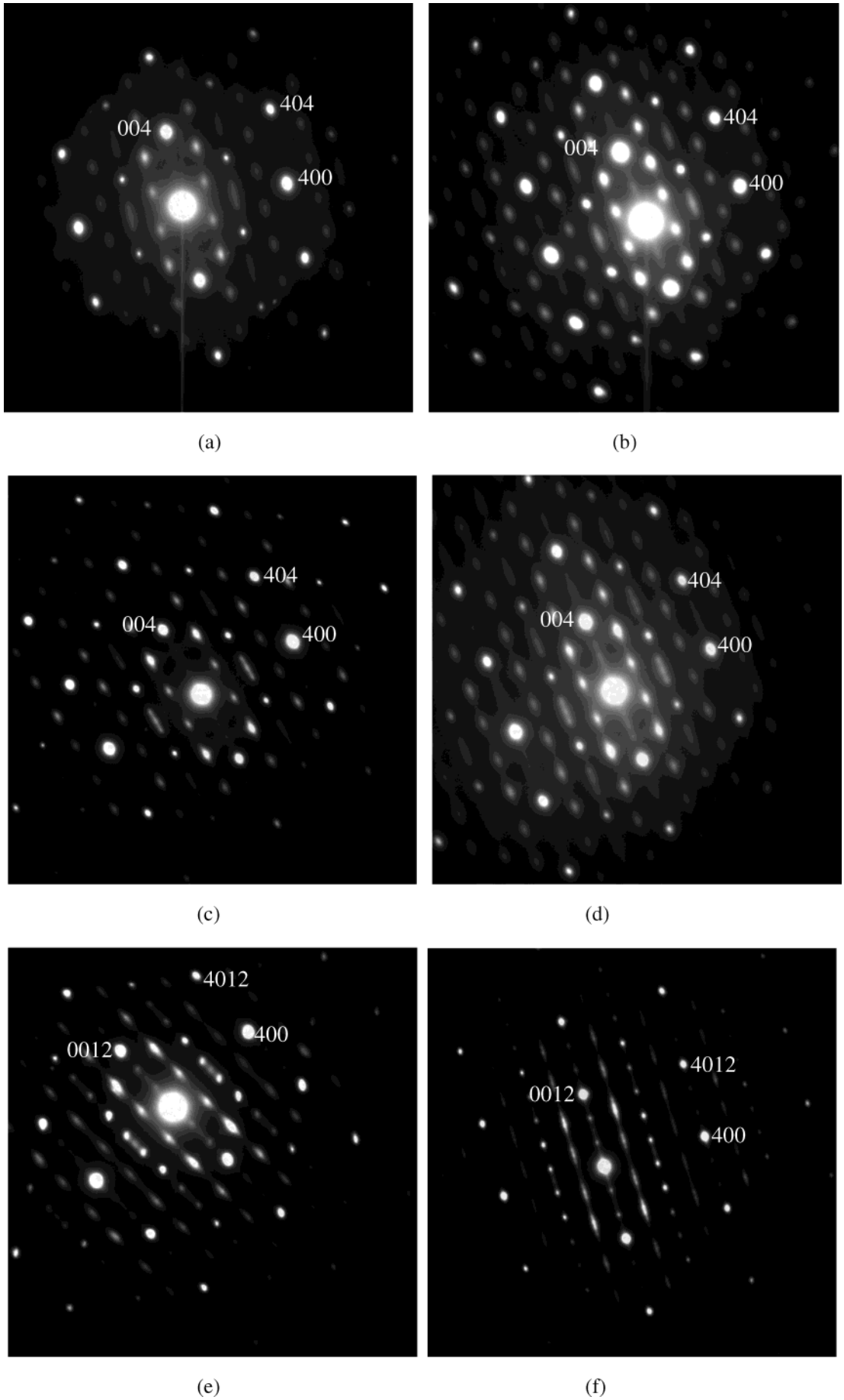

Figure 8. SAED patterns, looking down the [0*k*0] zone axis, for hydrogenated boehmite precalcined for 7 h at (a) 500, (b) 600, (c) 650, (d) 700, and (f) 900 °C.

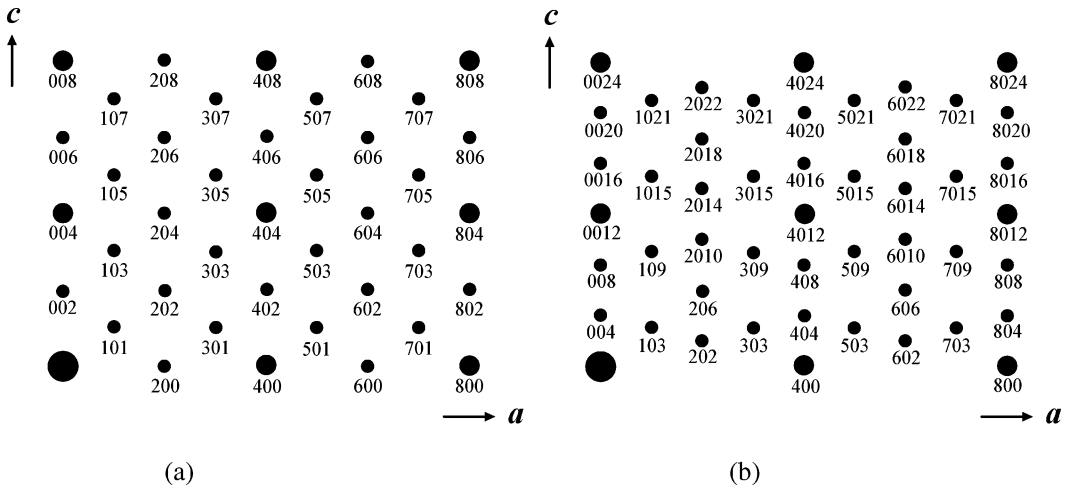

Figure 9. Indexing diagrams, using the $I4_1/amd$ space group, looking down the [0*k*0] zone axis, for (a) γ-Al_2O_3 and (b) γ'-Al_2O_3.

Table 1. Structural Parameters of Boehmite-Derived γ-Al_2O_3[a]

Space group $I4_1/amd$, $a = 5.616(4)$ Å, $c = 7.836(6)$ Å, $R_p = 3.08$, $\chi^2 = 1.96$, $R_B = 0.92$.					
site	*x*	*y*	*z*	*B* (Å^2)	occupancy
O (16*h*)	0	0.0102(50)	0.2535(60)	0.8(3)	1.0
Al (4*a*)	0	0.75	0.125	1.5(3)	0.75(2)
Al (8*c*)	0	0	0	1.6(3)	0.37(1)
Al (8*d*)	0	0	0.5	1.6(3)	0.59(1)

Core geometries (distances in Å, angles in °) around Al ions			
Al (4*a*)−O	1.774(46)		
Al (8*c*)−O	1.987(46)	2.027(21)	
Al (8*d*)−O	1.934(46)	1.946(21)	
O−Al(4a)−O	110.86(1.80)	108.86(91)	
O−Al(8*c*)−O	180.00	91.91(1.74)	88.09(1.74)
O−Al(8*d*)−O	180.00	92.02(1.80)	87.98(1.80)

[a] Data taken from the refinement of MRPD neutron data collected at room temperature from hydrogenated boehmite calcined at 600 °C for 7 h. Uncertainties are to three standard deviations.

diffuse than the sharpest peaks and are not as streaked as those from the tetrahedral sublattice. No reflections originate solely from the octahedral lattice but it has been deduced that it is more ordered than the tetrahedral sublattice and less ordered than the oxygen sublattice.[8] Reflection shapes, particularly from the *h*0*l*: $h + l = even$ reflections, were found to vary, indicating some disorder in the cation lattice. However, the oxygen lattice remains undisturbed with changing calcination temperature, consistent with the findings of other researchers.[28,29]

Streaking is attributed to stacking faults at cationic vacancies.[79] Variation in streak length with temperature represents change in the ordering of Al cations, synonymous with higher-order transformations.[43,44] The streaking of the *hkl*: $h + k + l = 2n$ reflections indicate vacancy ordering on tetrahedral positions in γ-Al_2O_3.[4] For δ-Al_2O_3, the reflections originating from planes with tetrahedral positions are sharp while those originating from planes with cations in variable coordination become sharp, indicating increased vacancy ordering on the octahedral sites only. A similar phenomenon is observed here for γ'-Al_2O_3 but vacancy ordering on tetrahedral positions is still evident. The diffuseness of the *h*0*l*: $h + l = even$ reflections in γ-Al_2O_3, which clearly increases with calcination temperature, suggests that vacancies are distributed among octahedral positions also. Vacancy distribution among octahedral and tetrahedral sites in γ-Al_2O_3 is also indicated by Rietveld refinements.[58] The measured coordination distribution from MAS NMR data provides further support for vacancies on octahedral and tetrahedral sites for both γ-Al_2O_3 and γ'-Al_2O_3.

Structural Details of γ-Alumina. The tetragonal model determined for γ-Al_2O_3 in previous work (Table 1) was most suitable to refine the data obtained here for γ-Al_2O_3.[58] The Cubic-16*c* model[58] (describes γ-Al_2O_3 by $Fd\bar{3}m$ symmetry using the Wyckoff 16*c* positions in addition to the spinel sites), and refinements of all structural models with interstitial hydrogen incorporated, were trialed at all temperatures between 500 and 750 °C (700 °C for the deuterated material). These structure refinements did not provide fits as good as the Tetragonal-8*c* model[58] ($I4_1/amd$ symmetry with the Wyckoff 8*c* positions incorporated into the model in addition to the spinel sites). Wilson and McConnell[44] also did not observe a cubic γ-Al_2O_3, attributing the absence to the process of vacancy ordering on octahedral sites which takes over and causes the increased tetragonal distortion that coincides with the next transition phase (δ-Al_2O_3 in their case).

Lattice expansion caused by the electron beam heating resulted in no observed trend from SAED patterns. The unit cell parameters were essentially constant, with respect to the inherent error associated with selected area electron diffraction. The measured *a* parameter

(79) Cowley, J. M. *Acta Crystallogr.* **1953**, *6*, 53.

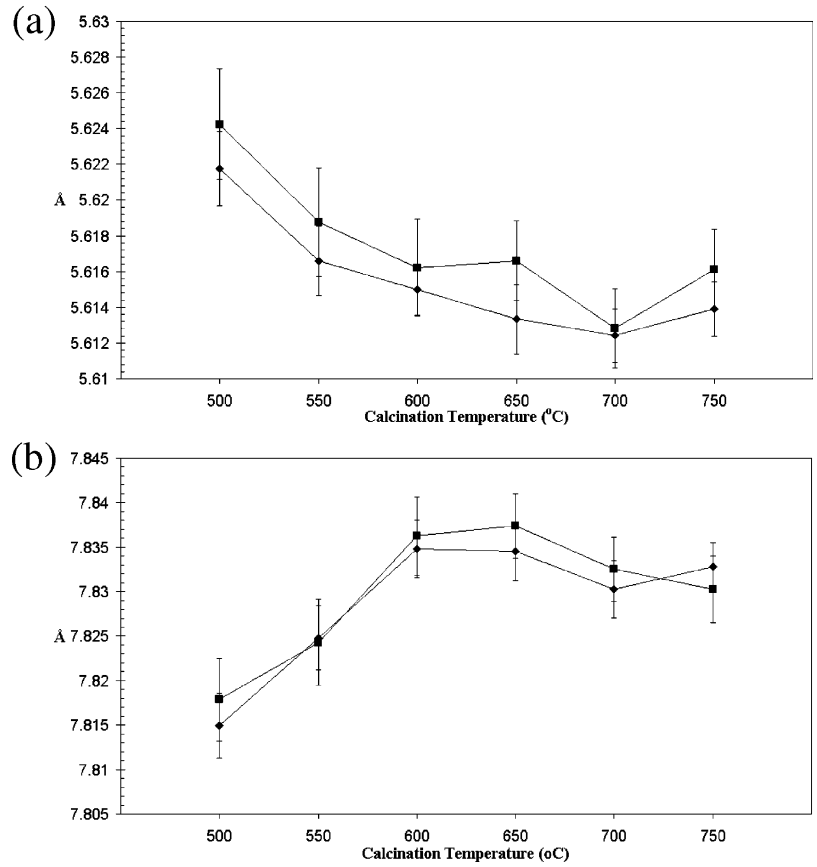

Figure 10. Variation in (a) *a* and (b) *c* parameters for γ-Al_2O_3 from Rietveld refinement of neutron diffraction data collected at room temperature from hydrogenated boehmite calcined for 7 h; ◆, HRPD; ■, MRPD.

was 5.70 ± 0.5 Å for both γ-Al_2O_3 and γ'-Al_2O_3. For γ-Al_2O_3 the *c* parameter was 8.0 ± 0.8 Å, and for γ'-Al_2O_3 it was 24.0 ± 2.3 Å.

Trends in the lattice parameters were observed from the neutron diffraction data. Figure 10 illustrates the change in lattice parameters with calcination temperature from room-temperature sample data. There is a small but definite increase in the *c* parameter until 600 °C, after which it remains effectively constant within the limits of the experimental uncertainty. This parameter corresponds to the contracted axis of cubic representations of tetragonally distorted γ-Al_2O_3 and the trend is consistent with these reports, i.e. that it coincides with reduced tetragonal distortion.[42−44] However, the *a* parameter also varies, initially decreasing before becoming effectively level after 600 °C. The net effect is constant volume within the limits of the uncertainties. For data collected during in situ heating there was a continuously increasing trend in cell volume due to the increasing thermal energy within the furnace.

Variation in the *y* coordinate of the oxygen sublattice asymmetric unit shows convergence of the coordinates with increasing calcination temperature to 650 °C (Figure 11). Because the data in Figure 11 represent the same material, and even though the uncertainties are large, the trend is significant. The convergence at 650 °C suggests increased ordering of the oxygen sublattice. By 700 °C the data diverge again as the splitting of the *hkl*: $h + k + l = 2n$ reflections commences and the γ'-Al_2O_3 phase becomes important. Beyond 700 °C the data begin to converge again as the ordering processes, which result in the γ'-Al_2O_3 structure, begin to dominate. Similar trends were observed for the *z* coordinate of the oxygen sublattice asymmetric unit. These trends also correspond with increased Bragg factors for Rietveld refinement of the γ-Al_2O_3 structure above 650 °C, as processes leading to γ'-Al_2O_3 become important.

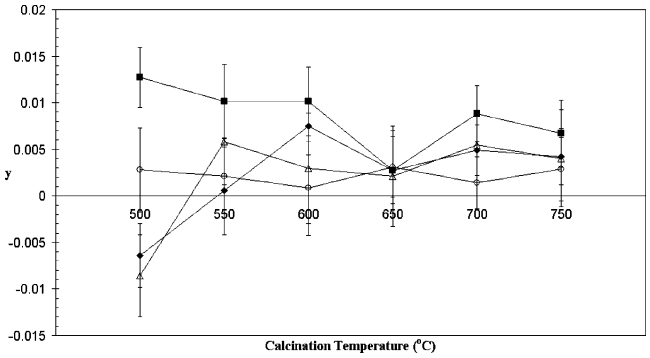

Figure 11. Variation in oxygen fractional *y* coordinate from Rietveld refinement of neutron diffraction data with calcination temperature for various samples: ◆, HRPD data collected from hydrogenated material at room temperature; ■, MRPD data collected from hydrogenated material at room temperature; and △ and ○, MRPD data collected during in situ heating from hydrogenated material.

The distribution of cations in octahedral and tetrahedral coordination obtained from Rietveld refinements was consistent with the MAS NMR data at each calcination temperature, with the proportion of cations on octahedral and tetrahedral sites always consistent within 3%. From the variation of occupancy with calcination temperature (Figure 12) greater fluctuation

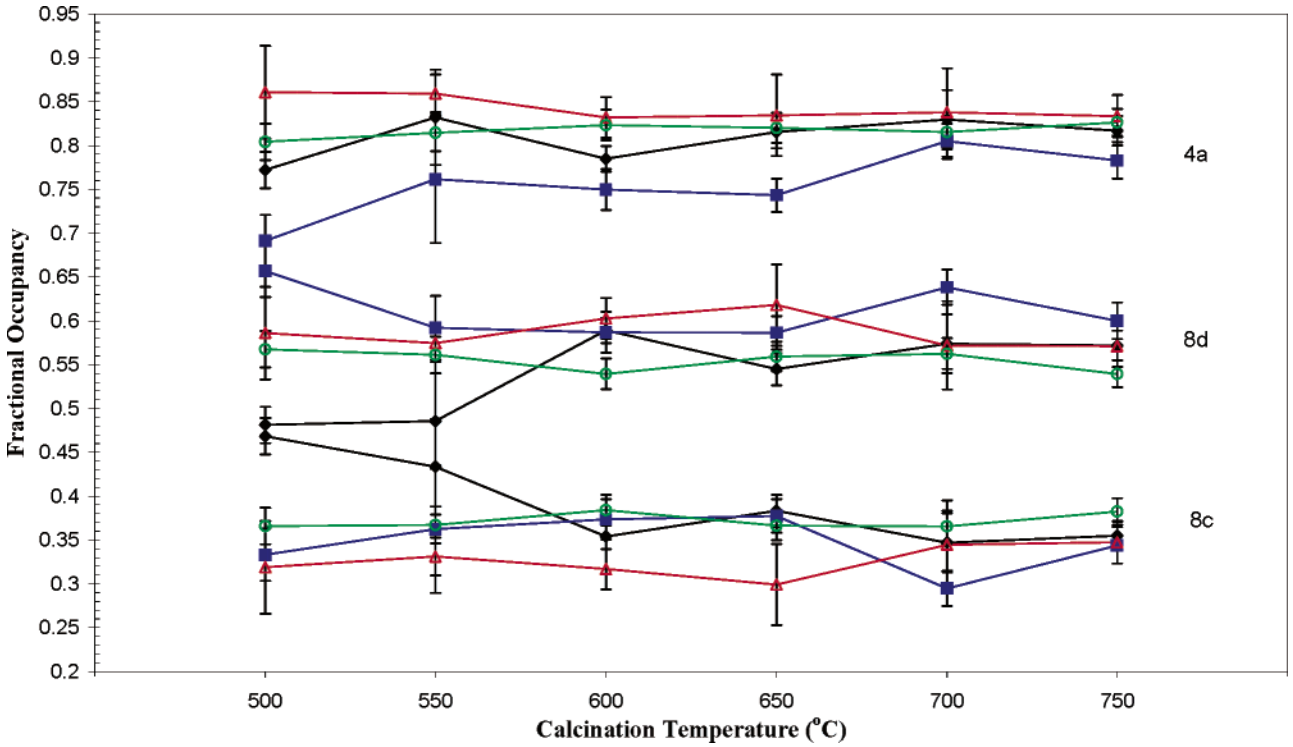

Figure 12. Variation in occupancy of octahedral (8*c* and 8*d*) and tetrahedral (4*a*) site positions from Rietveld refinement of neutron diffraction data with calcination temperature for various samples: ◆ (black), HRPD data collected from hydrogenated material at room temperature; ■ (blue), MRPD data collected from hydrogenated material at room temperature; and Δ (red) and ○ (green), MRPD data collected during in situ heating from hydrogenated material.

in the octahedral and tetrahedral site occupancies was observed at lower temperatures, suggesting a lower degree of order. For higher calcination temperatures the occupancy of tetrahedral sites tended to be constant, whereas changes in the ordering between the octahedral site positions was evident. An exception to the constant occupancies of tetrahedral sites was exhibited by the MRPD data obtained at room temperature: occupancy increased with calcination temperature, which coincides with the increased streaking observed in SAED patterns.

Insight into the causes of the tetragonal nature, and its reduction with higher calcination temperature, is provided by the observed changes in lattice parameters, coordinate position, and occupancy. Loss of water from the lattice has previously been suggested to cause the reduced tetragonal distortion.[42] Water loss is observed here, suggested by the lower background contributions observed with increasing calcination temperature in the neutron diffraction patterns. However, for water loss to be synonymous with the degree of tetragonal distortion, hydrogen must be present within the unit cell. Neutron data Rietveld refinements of the unit cell suggest that the presence of hydrogen is not likely within the bulk crystalline structure.[58] Also, from TEM (Figure 4), distinct amorphous regions were observed within the γ-Al_2O_3 grains, separate from the lamellar porous microstructures which constitute the crystalline structure. The structural water molecules are most likely to be present in these amorphous regions.

Lippens and De Boer[4] suggested the tetragonal distortion itself is due to shrinkage anisotropy of the lattice parameters during boehmite dehydration. Anisotropic change in the lattice parameters is also observed here after the formation of γ-Al_2O_3, and the lattice parameters become constant as the oxygen sublattice becomes more ordered (Figure 10).

It has also been proposed that the reduced tetragonal distortion is due to changes in cation ordering.[43,44] Variation in cation ordering is observed here (Figures 8 and 12). The unit cell of γ-Al_2O_3 is considered to be made up of the skeletal oxygen layers which remain intact after the OH layers of the boehmite precursor are broken down.[4,52,67] This leaves a cell with, initially, empty inter-skeletal layer regions. It is proposed that short-range ordering occurs within the unit cell whereby cations migrate into site positions within the inter-skeletal layers. The atoms within these regions will initially be rather disordered but increasingly become ordered as the structure evolves with higher temperature treatment. This inter-skeletal layer ordering would cause the variations in the oxygen sublattice seen here (Figure 11), which, in turn, causes the observed anisotropy in the lattice parameters followed by them becoming constant (Figure 10). More atoms migrate into the inter-skeletal layers as the structure evolves, with the proportion of octahedrally and tetrahedrally coordinated aluminum remaining constant, as per the MAS NMR spectra (Figure 5). This migration accounts for the variations in occupancy observed (Figure 12) as atoms move from one site position to another.

Determination of the Structure of γ'-Alumina. From the diffraction patterns above, cation ordering was more noticeable, and occurred over a shorter temperature range, for γ'-Al_2O_3. Similar to observations in the literature for δ-Al_2O_3,[43,44] the increase in tetragonal distortion in the neutron and X-ray diffraction patterns of γ'-Al_2O_3 coincided with the migration of vacancies to octahedral positions, as indicated by the SAED patterns.

Table 2. Structural Parameters of γ'-Al_2O_3 Formed by Calcination of Hydrogenated Boehmite Calcined at 800 °C for Seven Hours[a]

Space group $P\bar{4}m2$, $a = 5.611(3)$ Å, $c = 24.450(12)$Å, $R_p = 3.51$, $\chi^2 = 1.71$, $R_B = 1.01$						
	site	*x*	*y*	*z*	*B* (Å^2)	occupancy
	O(4*j*)	0.2334	0	0.1214	1.5	1.0
	O(4*j*)	0.2621	0	0.2965	1.5	1.0
	O(4*j*)	0.2470	0	0.4572	1.5	1.0
	O(4*j*)	0.2342	0	0.6255	1.5	1.0
	O(4*j*)	0.2294	0	0.7982	1.5	1.0
	O(4*j*)	0.2548	0	0.9581	1.5	1.0
	O(4*k*)	0.2334	0.5	0.1157	1.5	1.0
	O(4*k*)	0.2621	0.5	0.2965	1.5	1.0
	O(4*k*)	0.2470	0.5	0.4572	1.5	1.0
	O(4*k*)	0.2342	0.5	0.6255	1.5	1.0
	O(4*k*)	0.2294	0.5	0.7904	1.5	1.0
	O(4*k*)	0.2548	0.5	0.9581	1.5	1.0
T	Al(2*e*)	0	0	0.2620	1.1	0.25
T	Al(2*f*)	0.5	0.5	0.0882	1.1	0.75
T	Al(2*f*)	0.5	0.5	0.1816	1.1	1.0
T	Al(2*f*)	0.5	0.5	0.4194	1.1	1.0
T	Al(4*i*)	0.2518	0.2513	0.5	1.1	0.25
T	Al(8*l*)	0.2590	0.2546	0.1703	1.1	0.375
T	Al(8*l*)	0.2510	0.2513	0.3297	1.1	0.125
O	Al(4*j*)	0.2490	0	0.1987	1.1	0.75
O	Al(4*j*)	0.2457	0	0.3751	1.1	1.0
O	Al(4*j*)	0.2530	0	0.5536	1.1	0.25
O	Al(4*j*)	0.2457	0	0.8811	1.1	0.5
O	Al(4*k*)	0.2680	0.5	0.0331	1.1	0.125
O	Al(4*k*)	0.2590	0.5	0.2108	1.1	0.5
O	Al(4*k*)	0.2506	0.5	0.3759	1.1	0.875
O	Al(4*k*)	0.2562	0.5	0.7106	1.1	1.0
O	Al(4*k*)	0.2512	0.5	0.8861	1.1	0.25

[a] Data were collected at room temperature using MRPD. Uncertainties are to three standard deviations. All uncertainties, where not stated otherwise, are 0.005 for refinable coordinate positions and 0.3 for thermal parameters.

Table 3. Aluminum−Oxygen Bond Lengths (Å) and Angles (°) for γ'-Al_2O_3 Formed by Calcination of Hydrogenated Boehmite Calcined at 800 °C for Seven Hours

Al(2e)−O	1.678	1.910		
Al(2f)−O	1.630	1.752		
Al(2f)−O	1.654	2.150		
Al(2f)−O	1.666	1.834		
Al(4i)−O	1.725			
Al(8l)−O	1.590	1.682	1.813	1.901
Al(8l)−O	1.609	1.750		
Al(4j)−O	1.815	1.901	1.925	2.294
Al(4j)−O	1.846	1.905	1.924	1.940
Al(4j)−O	1.691	1.976	1.999	2.260
Al(4j)−O	1.833	1.902	1.921	1.939
Al(4k)−O	1.757	1.905	1.949	2.048
Al(4k)−O	2.009	2.033	2.112	2.235
Al(4k)−O	1.725	2.044	2.048	2.052
Al(4k)−O	1.878	1.919	1.969	1.999
Al(4k)−O	1.832	2.049	2.056	2.104
O−Al(2e)−O	122.38	84.74		
O−Al(2f)−O	133.27	103.46		
O−Al(2f)−O	133.21	88.20		
O−Al(2f)−O	116.92	108.80		
O−Al(4i)−O	109.81	108.82		
O−Al(8l)−O	117.40	101.09		
O−Al(8l)−O	107.53	106.30		
O−Al(4j)−O	179.08	94.57	89.18	
O−Al(4j)−O	176.93	93.72	90.61	
O−Al(4j)−O	175.57	99.83	89.78	
O−Al(4j)−O	177.81	91.44	89.54	
O−Al(4k)−O	171.88	97.91	94.05	90.33
O−Al(4k)−O	176.80	96.08	91.90	81.72
O−Al(4k)−O	178.42	94.40	93.22	87.46
O−Al(4k)−O	171.87	92.38	91.49	87.54
O−Al(4k)−O	178.10	95.08	91.37	86.79

[a] Uncertainties are to three standard deviations. All uncertainties, where not stated otherwise, are 0.008 for distances and 0.05 for angles.

The Rietveld refined model of γ-Al_2O_3 was capable of modeling the data for γ'-Al_2O_3, but because of the physical differences known to exist between these materials it would have been incorrect to follow this path. Determination of the unit cell structure of γ'-Al_2O_3 proceeded by considering a trial structure model, consisting only of oxygen ions as a triple cell of γ-Al_2O_3, as indicated by the SAED results. On the basis of a physically meaningful distribution and the size of the site positions, a number of octahedral and tetrahedral positions were trialed. The refinements presented here represent the best trials (Tables 2−5). An example of a refinement fit is shown in Figure 13. From indexing, the oxygen sublattice configuration, and the Al distribution, it became apparent that γ'-Al_2O_3 was represented in the $P\bar{4}m2$ space group. Refinements under this space group best preserved the oxygen lattice while allowing the cations to become more ordered with respect to the γ-Al_2O_3 precursor. The unit cell dimensions and space group obtained are similar to that determined for δ-Al_2O_3 by Repelin and Husson.[57] Both the 800 and 900 °C data refinements yielded 66(3)% octahedral and 34(3)% tetrahedral Al cation coordination. This is in agreement with the MAS NMR data and supports the plausibility of these structural models.

Unlike γ-Al_2O_3, the change in the ordering of the sites is obvious when looking directly at the Rietveld structure models of γ'-Al_2O_3 between 800 and 900 °C (Tables 2−5). Cations in octahedral sites are considerably disordered, which is a consequence of the rapid change in the structure of γ'-Al_2O_3 with increasing temperature treatment. It therefore appears that γ'-Al_2O_3 can be considered as a series of transition states within the γ-Al_2O_3 to θ-Al_2O_3 transformation.

A reduced number of occupied site positions were observed with increasing temperature. At 800 °C there are some symmetry-equivalent positions with low occupancy. These low occupancies occur as a result of symmetry. This is to say that occupied symmetry-equivalent site positions in close proximity to each other have low occupancies to maintain physically reasonable average interatomic distances. The atoms were generally found to migrate from symmetry positions with low occupancy to other sites with higher occupancy. By 900 °C the structure is again more ordered with a reduced number of octahedral and tetrahedral sites occupied by cations. The number of occupied site positions approaches that of the δ-Al_2O_3 model of Repelin and Husson.[57] Also at 900 °C, one of the octahedral positions, at (0.1353, 0.5, 0.0013), appears significantly distorted to warrant its consideration as atoms migrating from octahedral to tetrahedral positions. These observations are consistent with the observation by SAED that at 900 °C the structure appears to be approaching that of δ-Al_2O_3.

Conclusions

The evolution in the structure of γ-Al_2O_3, derived from well-crystalline boehmite, calcined at various temperatures in air was investigated. Tetragonal γ-Al_2O_3 was found to be present between 450 and 750 °C. The

Table 4. Structural Parameters of γ'-Al_2O_3 Formed by Calcination of Hydrogenated Boehmite Calcined at 900 °C for Seven Hours[a]

Space Group $P\bar{4}m2$, $a = 5.617(3)$ Å, $c = 24.405(12)$ Å, $R_p = 4.03$, $\chi^2 = 2.13$, $R_B = 1.70$						
	site	*x*	*y*	*z*	*B* (Å^2)	occupancy
	O(4*j*)	0.2394	0	0.1223	1.1	1.0
	O(4*j*)	0.2708	0	0.2922	1.1	1.0
	O(4*j*)	0.2430	0	0.4566	1.1	1.0
	O(4*j*)	0.2302	0	0.6214	1.1	1.0
	O(4*j*)	0.2298	0	0.7975	1.1	1.0
	O(4*j*)	0.2444	0	0.9575	1.1	1.0
	O(4*k*)	0.2394	0.5	0.1191	1.1	1.0
	O(4*k*)	0.2708	0.5	0.2951	1.1	1.0
	O(4*k*)	0.2430	0.5	0.4566	1.1	1.0
	O(4*k*)	0.2302	0.5	0.6214	1.1	1.0
	O(4*k*)	0.2298	0.5	0.7897	1.1	1.0
	O(4*k*)	0.2444	0.5	0.9575	1.1	1.0
T	Al(2*e*)	0	0	0.3300	0.8	0.375
T	Al(2*f*)	0.5	0.5	0.0882	0.8	0.5
T	Al(2*f*)	0.5	0.5	0.1816	0.8	1.0
T	Al(2*f*)	0.5	0.5	0.4200	0.8	1.0
T	Al(4*i*)	0.2518	0.2513	0.5	0.8	0.1875
T	Al(8*l*)	0.2588	0.2546	0.1703	0.8	0.5625
O	Al(4j)	0.2490	0	0.1987	0.8	0.5
O	Al(4j)	0.2457	0	0.3751	0.8	1.0
O	Al(4j)	0.2457	0	0.8810	0.8	0.6875
O	Al(4k)	0.2590	0.5	0.2108	0.8	0.625
O	Al(4k)	0.2506	0.5	0.3759	0.8	1.0
O	Al(4k)	0.2562	0.5	0.7106	0.8	1.0
O	Al(4k)	0.1353	0.5	0.0013	0.8	0.4375

[a] Data were collected at room temperature using MRPD. Uncertainties are to three standard deviations. All uncertainties, where not stated otherwise, are 0.005 for refinable coordinate positions and 0.3 for thermal parameters.

Table 5. Core Geometries (Distances in Å, Angles in °) around Al Ions for γ'-Al_2O_3 Formed by Calcination of Hydrogenated Boehmite Calcined at 900 °C for Seven Hours[a]

Al(2e)−O	1.722	1.760		
Al(2f)−O	1.633	1.790		
Al(2f)−O	1.660	2.069		
Al(2f)−O	1.679	1.799		
Al(4i)−O	1.733			
Al(8l)−O	1.598	1.799	1.847	1.692
Al(4j)−O	1.789	1.905	1.931	2.192
Al(4j)−O	1.893	1.908	1.929	1.945
Al(4j)−O	1.813	1.962	1.928	1.933
Al(4k)−O	1.973	2.034	2.112	2.150
Al(4k)−O	1.758	2.028	2.078	2.074
Al(4k)−O	1.857	1.884	1.932	2.093
Al(4k)−O	1.194	1.889	2.366	2.681
O−Al(2e)−O	119.68	97.33		
O−Al(2f)−O	127.37	106.69		
O−Al(2f)−O	132.23	90.07		
O−Al(2f)−O	118.59	114.81		
O−Al(4i)−O	112.33	107.81		
O−Al(8l)−O	115.90	102.13		
O−Al(4j)−O	178.50	94.40	91.41	89.70
O−Al(4j)−O	176.29	94.60	87.20	
O−Al(4j)−O	178.61	92.56	89.54	86.48
O−Al(4k)−O	178.99	96.61	91.60	89.07
O−Al(4k)−O	177.49	98.08	93.65	85.25
O−Al(4k)−O	173.80	97.39	88.87	
O−Al(4k)−O	98.92	95.21	81.87	

[a] Uncertainties are to three standard deviations. All uncertainties, where not stated otherwise, are 0.008 for distances and 0.05 for angles.

structure showed a reduction in the tetragonal distortion with increasing temperature but at no stage was cubic γ-Al_2O_3 obtained. Examination of the progress of cation migration indicates the reduction in the tetragonal nature is due to ordering within inter-skeletal oxygen layers of the unit cell, left over from the breakdown of the hydroxide layers of boehmite when the transformation occurred.

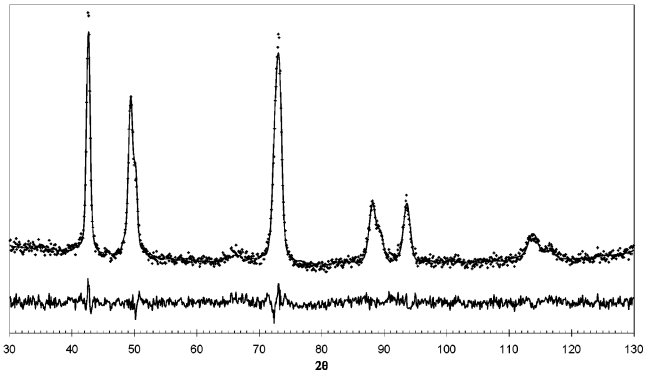

Figure 13. Rietveld refinement for γ'-Al_2O_3 formed by calcination of hydrogenated boehmite calcined at 800 °C for 7 h.

Above 750 °C, δ-Al_2O_3 was not observed, but a new phase was identified and designated γ'-Al_2O_3. The structure of this phase was determined to be a triple cell of γ-Al_2O_3 and is herein described using the $P\bar{4}m2$ space group. The cation ordering is more obvious in this structure, with fewer site positions being occupied with increasing calcination temperature. Hence, the structure of γ'-Al_2O_3 may be considered as a series of transition states within the γ-Al_2O_3 to θ-Al_2O_3 transformation. Some distorted cation positions indicate the onset of migration from octahedral to tetrahedral sites at 900 °C, where the structure approaches the appearance of δ-Al_2O_3.

Consistent cation coordination, of ∼69% octahedral and ∼31% tetrahedral, was observed from MAS NMR spectra of material calcined at temperatures between 500 and 900 °C. These values agree with the cations in octahedral and tetrahedral coordination obtained in the Rietveld refinements, supporting the physical integrity of the structure models.

Neutron data Rietveld refinements of the structural models suggest that hydrogen is not present within the bulk crystalline structure of any of the calcination products. Amorphous regions, where hydrogen in the bulk is most likely to reside, were observed in TEM micrographs. No obvious variations were found in the lamellar porous microstructure and diffraction patterns observed for the calcination products obtained between 500 and 700 °C, and between 800 and 900 °C, for different preparation routes used.[44] The consideration of hydrogen in the structure will be detailed in the second part of this paper to be published separately.[73]

Acknowledgment. G.P. acknowledges the Australian government for an Australian Post Graduate Award with Stipend (APAWS) to fund this research. G.P. is also grateful to the Australian Institute of Nuclear Science and Engineering (AINSE) for the provision of access to the facilities at ANSTO and an AINSE Post-Graduate Research Award (APGRA). G.P. also thanks the Western Australian Interactive Virtual Environments Centre (IVEC) for provision of an IVEC Doctoral Scholarship (WAIDS). Special thanks to Professor Brian O'Connor of Curtin University of Technology, and Dr. Lindsay Byrne of the University of Western Australia, who

provided valuable assistance and very useful advice. Thanks to Kristy Blyth, Curtin University of Technology, for performing the DTA−TGA experiment and John Cornell of Alcoa World Alumina, Western Australia, for providing hydrogenated boehmite powder.
CM034917J